



HAL
open science

Nominal Bias Analysis for ARAIM User

Christophe Macabiau, Carl Milner, Alexandre Chabory, Norbert Suard,
Catalina Rodriguez, Mikaël Mabillean, Jonathan Vuillaume, Sixtine Hegron

► **To cite this version:**

Christophe Macabiau, Carl Milner, Alexandre Chabory, Norbert Suard, Catalina Rodriguez, et al..
Nominal Bias Analysis for ARAIM User. ION International Technical Meeting 2015, Institute of
Navigation, Jan 2015, Dana Point, United States. hal-01145811

HAL Id: hal-01145811

<https://enac.hal.science/hal-01145811>

Submitted on 27 Apr 2015

HAL is a multi-disciplinary open access archive for the deposit and dissemination of scientific research documents, whether they are published or not. The documents may come from teaching and research institutions in France or abroad, or from public or private research centers.

L'archive ouverte pluridisciplinaire **HAL**, est destinée au dépôt et à la diffusion de documents scientifiques de niveau recherche, publiés ou non, émanant des établissements d'enseignement et de recherche français ou étrangers, des laboratoires publics ou privés.

Nominal Bias Analysis for ARAIM User

C. Macabiau, C. Milner, A. Chabory, *ENAC*
N. Suard, C. Rodriguez, *CNES*
M. Mabillean, J. Vuillaume, S. Hegron, *EGIS-AVIA*

BIOGRAPHIES

Christophe MACABIAU graduated as an electronics engineer in 1992 from the ENAC (Ecole Nationale de l'Aviation Civile) in Toulouse, France. Since 1994, he has been working on the application of satellite navigation techniques to civil aviation. He received his Ph.D in 1997 and has been in charge of the signal processing lab of ENAC since 2000, where he also started dealing with navigation techniques for urban navigation. He is currently the head of the TELECOM lab of ENAC, which includes research groups on signal processing and navigation, electromagnetics and data communication networks.

Carl MILNER is an Assistant Professor within the Telecom Lab at the Ecole Nationale Aviation Civile. He has a Master's degree in Mathematics from the University of Warwick, a PhD in Geomatics from Imperial College London and has completed the graduate trainee programme at the European Space Agency. His research interests include GNSS augmentation systems, integrity monitoring, air navigation and applied mathematics.

Alexandre CHABORY graduated in 2001 as an electronics engineer from the French Civil Aviation University (ENAC). From 2001 to 2004, he was a PhD student with ONERA. From 2004 to 2007, he was a postdoctoral scientist with the Eindhoven University of Technology (TU/e). Since 2007, he is an assistant professor with the Electromagnetics and Antennas Research Group of the Telecom lab of ENAC. His research interests mainly deal with electromagnetic theory, modeling and applications.

Norbert SUARD joined the CNES in 1983. He is a Senior Expert in the CNES Navigation System Division where he has over 25 years of experience in development, studies, performances analysis of navigation system augmentation like CE-GPS, EURIDIS, ESTB and now EGNOS, WAAS and GAGAN. He is currently more specifically in charge of the CNES Navigation and Time Monitoring Facility (NTMF) designed to monitor GPS and SBAS Signals In Space and Performances, He is member of the WGC of the UE-US agreement in the promotion, provision and use of civil GPS and GALILEO navigation and timing signals and services.

Catalina RODRIGUEZ graduated as an electronic engineer from CNAM in Paris. She worked at Thales Alenia Space as a Navigation System Engineer on EGNOS and joined CNES in 2005. Today integrated within ESA's EGNOS project team, she is involved in many activities linked to SBAS standardisation and EGNOS extensions.

Mikael MABILLEAU graduated from ENAC and has integrated Egis Avia as CNS project Engineer. He has been involved since 2006 in Galileo standardisation activities for Civil Aviation. He follows the standardisation activities of the EUROCAE WG 62 and ICAO NSP group (Navigation System Panel). Mikael led a subgroup of the WG62 in charge of the standardisation of Galileo integrity in 2009 (RAIM, GIC). He is also managing the CNES project initiatives on Advanced RAIM and SBAS L1L5 proposition of standard as well as the EUROCONTROL ionosphere project.

Jonathan VUILLAUME is an ENAC engineer, who joined Egis Avia to carry out navigation studies. Currently, Jonathan is working on projects dealing with GPS augmentation systems and Galileo integrity monitoring. Then, he also participates in projects linked to the new ARAIM concept and to the definition of innovative integrity concepts for SBAS. He has recently implemented an operational tool to assess iono disturbances effect on GPS augmentation system, ABAS and GBAS.

Sixtine HEGRON is an engineer in apprenticeship at the ENAC in Toulouse and has joined Egis Avia in 2013.

ABSTRACT

Receiver Autonomous Integrity Monitoring (RAIM) has been certified to provide lateral guidance in flight operations ranging from En-route to Non-Precision Approach (NPA). Recent developments in the RAIM algorithm science, namely Advanced RAIM (ARAIM), have suggested a future role in vertically guided operations down to LPV with a decision height of 200ft [EU-U.S., 2012]. However, more stringent requirements as a result of the vertical guidance application question the external risk or trust that is placed on the constellation service provision and may require the partial reduction of this risk through the use of a ground segment, identifying and removing threats and providing data through an ISM

(Integrity Support Message). This ground segment should ideally be light and low-cost so not to replicate that implemented for SBAS. In addition the ISM latency [Walter et al, 2012] should ideally be allowed as long as possible to obviate the challenging and expensive communications requirements as imposed, for example, on SBAS (6 sec Time to Alert). Furthermore, the ISM should be as simple as possible to ensure the data broadcast requirements can be met with a number of solutions from ATC, to local ground communications to GEO relay. Finally, the network should be light, in the sense of a sparse and global distribution of stations.

In order to meet the defined role of the ground segment and its monitoring capability; three possible methodologies were identified [Milner et al, 2014]: No ground monitoring, Offline Monitoring, Real-Time Monitoring.

The parameters of interest to this monitoring are the input parameters defined for the ARAIM baseline airborne algorithm as given below:

- URA/SISA: Standard deviation of ranging measurement for integrity
- URE/SISE: Standard deviation of ranging measurement for nominal accuracy/continuity
- Bnom: Maximum nominal bias on ranging measurement
- P_{sat}: Prior probability of fault in satellite per approach
- P_{const} : Prior probability of fault affecting more than one satellite in constellation per approach

This list of parameters contains the maximum nominal bias Bnom. A nominal bias is a fault-free bias, both to account for near-constant uncorrected errors (signal deformation and antenna bias) and non-Gaussian behaviour. However, some small nominal bias may be included in this Bnom parameter.

Indeed, after application of all possible corrections, iono-free smoothed code ranges are affected by residual ephemeris plus satellite clock and payload group delay errors w.r.t constellation reference frame and clock. In the context of ARAIM, the residual ephemeris plus clock errors, residual tropospheric error, and multipath plus noise errors, are all assumed to be random errors overbounded by zero mean gaussian errors with known modeled variance. However, it is noted that the residual ephemeris plus satellite clock errors may include a long term bias.

These ionofree smoothed code ranges are also affected by the receiver clock offset, defined as the common propagation delays from antenna to signal processing stages, also defined as the error identical to all measurements of the same constellation, which varies across constellations (time reference, signal) and the receiver design. Note that the receiver clock offset may include residual payload plus ephemeris delays identical to all satellites used in the navigation solution

computation, so may vary depending on the set of satellites used in this computation.

The iono-free nominal bias may then be defined as the permanent bias in excess of the residual error identical to all measurements of the same constellation, and from this definition may therefore depend on the receiver clock offset.

A first paper has been issued to define properly the nominal bias and to characterize over the globe those biases for an ARAIM user [Macabiau et al, 2014]. Three possible types of sources of nominal bias were identified: nominal signal deformation, variation of SV antenna group delay with nadir angle, variation of user antenna group delay with Azimuth (Az) and Elevation (El) angles. Models used to characterize these nominal bias contributions were proposed and fully defined. Assumptions were made at several levels of these models to try and reflect possible nominal situations of signal distortion, SV or user receiver antenna group delay variation. Initial work was presented on the ARAIM reference algorithm integrity monitoring performance to protect the ARAIM user against the impact of these nominal biases, driven by the ISM input Bnom value transmitted by the ground segment.

The aim of this paper is therefore to update the analysis done on nominal bias affecting the ARAIM user, on the capacity of the ground monitoring network to provide a pertinent Bnom, and on the impact on the ARAIM user performance. This methodology allows determining possible restrictions on ARAIM user receiver characteristics.

Based on the definition of the ARAIM user nominal bias expressed in [Macabiau et al, 2014] identifying three possible sources of nominal bias (signal deformations, SV antenna, and user antenna), assumption and models definition are set in the first part of the paper. Then, we determine the impact of that defined nominal bias on the ARAIM user receiver range measurement and position estimate. Impact of nominal signal deformations is evaluated using a model derived from the bounding ICAO EWF threat model. The evaluation considers different receiver configurations in terms of bandwidth and chip spacing, representing the regions that are proposed at RTCA/EUROCAE [Phelts et al., 2014b] plus regions identified to induce a maximum ranging error due to nominal signal deformation. The analysis of the nominal bias obtained for the different configuration leads to the identification of suitable design requirements for the ARAIM user receiver. Impact of user antenna group delay variation as a function of Azimuth and Elevation is then addressed, considering several models for user antenna, including recent results for the model of a dual-frequency civil aviation antenna mounted on aircraft. Impact of SV antenna group delay variation is also assessed based on mathematical analysis of antenna group delay. Then, through simulation, we analyze the results of

the implementation of these ground monitoring techniques for estimation of the B_{nom} bounds and we analyze the performance of these bounds with respect to the possible distribution of the ARAIM user nominal bias. Situations leading to extreme integrity situations have been identified and are analyzed with respect to current monitoring concept used in the ISM. This analysis will assess the sensitivity of the results with respect to the model used to define each nominal bias contributor. From these simulations, we finally conclude on the capacity of the ground to provide efficient B_{nom} coupled with some possible restrictions for the characteristics of the ARAIM user receiver.

INTRODUCTION

ARAIM user Rx pseudorange measurements are affected by slowly varying range errors, called nominal biases, not fully corrected by the Constellation Service Provider (CSP) navigation message or by the ARAIM Integrity Support Message (ISM), and only partially reflected by the ARAIM ISM URE. The reason why these long term biases affect differently a ground segment and the user receiver is due to the differences in the ground segment receiver sites and user receiver (location, antenna, receiver).

In addition to the ARAIM ISM URE, this ARAIM receiver uses input ISM B_{nom} values reflecting nominal biases, and ISM URE and B_{nom} are used for fault detection test and computation of protection levels. CNES therefore felt interesting to analyze requirements for the ARAIM ground segment to provide an adequate ISM so that the impact of nominal biases on ARAIM user performance is acceptable, and launched a project carried out by EGIS-AVIA and ENAC. One important issue is the possible constraints on ARAIM ground and user segment to reach a specific performance (ex: BW, Cs region).

DEFINITION OF NOMINAL BIASES

The section 1 of the Milestone I report on ARAIM Working Assumptions [EU-US, 2012] provides some definitions about ARAIM user receiver nominal biases that could be used as baseline in the framework of ARAIM activity. In particular, the User Range Error (URE) is the standard deviation error corresponding to system accuracy and continuity performance. For ARAIM, this error will not account for fault bias errors. However, small nominal biases may be included in this parameter. This Milestone I report on ARAIM [EU-US, 2012] also mentions the definition of nominal bias in range measurements by noting that the GEAS Phase II report [FAA, 2010] allowed for the possibility of fault-free biases, both to account for near-constant uncorrected errors (signal deformation and antenna biases) and non-Gaussian behaviour. It also defines the fault-free case as the case that covers the causes of HMI that are due to large random errors that can occur with small probability in the normal operation of the system, such as those

caused by receiver noise, multipath and inaccurate tropospheric delay estimation along with an unfortunate combination of bias errors.

This report also mentions that the systematic error due to antenna bias can be accounted for within the maximum nominal bias term to be broadcast to ARAIM users. These biases depend on the look angle of the signal through the antenna and may be different for each frequency and for code and carrier.

GEAS Phase II report [FAA, 2010] also notes that alert limits for LPV-200 are fairly small compared to those for LNAV approach. As such, the effect of small range errors due to several sources (e.g., errors due to nominal signal deformations, antenna biases) cannot be ignored when analyzing the integrity performance of the algorithm. These small range errors include errors that remain essentially constant throughout the duration of an approach, and therefore cannot be treated as if they were purely random (i.e., uncorrelated over periods of time of 15 seconds or more).

However, we feel that it would be useful to clarify the definition of these ARAIM user receiver nominal biases in order to identify clear techniques for determination of appropriate bounds on their value such as they are used inside the ARAIM user receiver algorithm, and to determine the ARAIM user performance induced by the value of these bounds.

The ionofree GNSS pseudorange measurements in a multi-constellation GPS/GALILEO dual frequency ARAIM receiver, corrected by all possible corrections (CSP navigation message satellite clock and Tgd as appropriate, possible online ARAIM ISM clock correction from online ISM navigation message overlay if online ARAIM is used, relativistic effect, ARAIM user tropospheric error) could be modeled as proposed hereafter:

$$P_{L1-L5}(k) = \frac{f_{L1}^2}{f_{L1}^2 - f_{L5}^2} P_{L1}(k) + \frac{f_{L5}^2}{f_{L5}^2 - f_{L1}^2} P_{L5}(k)$$

$$P_{E1-E5a}(k) = \frac{f_{E1}^2}{f_{E1}^2 - f_{E5a}^2} P_{E1}(k) + \frac{f_{E5a}^2}{f_{E5a}^2 - f_{E1}^2} P_{E5a}(k)$$

$$\frac{f_{L1}^2}{f_{L1}^2 - f_{L5}^2} = \frac{f_{E1}^2}{f_{E1}^2 - f_{E5a}^2} \approx 2.261$$

$$\frac{f_{E5a}^2}{f_{E5a}^2 - f_{E1}^2} = \frac{f_{L5}^2}{f_{L5}^2 - f_{L1}^2} \approx -1.261$$

These iono-free code measurements are then smoothed with iono-free phase measurements.

The final smoothed ionofree measurements would therefore be modeled as:

$$P^{GPSi} = \sqrt{(x - x^i)^2 + (y - y^i)^2 + (z - z^i)^2} + \delta\rho^i + b^{GPS} - \delta d^{GPSi} + \delta\tau^i + mult^i + n^i + b^{GPSi}$$

$$P^{GALj} = \sqrt{(x - x^j)^2 + (y - y^j)^2 + (z - z^j)^2} + \delta\rho^j + b^{GAL} - \delta d^{GALj} + \delta\tau^j + mult^j + n^j + b^{GALj}$$

where x^i , y^i , z^i are the satellite positions computed by the user receiver using the CSP navigation message and

possibly the online ARAIM navigation message overlay if online ARAIM is used.

In this model, the range residual quantities involved are described below:

- $\delta\rho^i - \delta d^{GPSi}$ is the sum of residual range error due to ephemeris error and satellite clock error w.r.t the CSP reference frame and CSP clock reference. Note that in the case of GPS L1/L5 ionofree measurement, this residual error also includes the error affecting the broadcast $T_{GD L1/L5}$ as the GPS ground segment monitors the L1/L2 iono-free measurements. In the context of ARAIM, this residual error is assumed to be random, with a distribution overbounded by a Gaussian distribution with zero mean and standard deviation termed URE. This residual error may include a long term bias of a few hours reflecting the rhythm of the ODS output, assumed to be included in URE.
- $\delta\tau^i$, $mult^i + n^i$ are the residual tropospheric and multipath plus noise errors. They are assumed by the ARAIM receiver algorithm to be random errors with a distribution overbounded by a 0 mean gaussian error with variance modeled as σ_{tropo}^2 , σ_{mult}^2 , σ_{noise}^2 .
- b^{GPS} , b^{GAL} are the ARAIM receiver clock offset with respect to GPS reference time and GALILEO reference time. These clock offsets should include all propagation delays common to all satellites of the same constellation from user antenna reference center point to signal processing module. This offset represents the error term which is identical to all measurements of the same constellation. Note that from this definition the receiver clock offset may include payload, plus ephemeris or SV clock delays identical to all satellites of the same constellation used, so it may vary depending on the set of satellites used.
- b^{GPSi} , b^{GALj} are the iono-free nominal biases for GPS satellite i, and GALILEO satellite j. Each quantity is a bias with long-term variation that is not reflected in the URE. It may include an average component identical to all measurements of the same constellation. This identical component may also be included in the receiver clock offset

The nominal range bias is seen primarily as a permanent bias equal to the bias due to nominal signal deformations affecting the user receiver, minus the bias due to the same nominal signal deformation affecting the CSP ground segment receivers (and possibly the ARAIM ground segment receivers in the case of online ARAIM). It may also include an additional component that is a bias due to the variation of the SV antenna group delay with the pointing angle towards the used. In addition, it may also include an additional bias due to user antenna group delay variation with azimuth and elevation of the direction of arrival of the satellite signal.

MODEL OF NOMINAL BIASES

In the general case, this nominal bias may therefore be modeled as:

$$b^{GPSi} = \frac{f_{L1}^2}{f_{L1}^2 - f_{L5}^2} (bsig_{L1}^{GPSi} + bSV_{L1}^{GPSi} + bant_{L1}^{GPSi}) + \frac{f_{L5}^2}{f_{L5}^2 - f_{L1}^2} (bsig_{L5}^{GPSi} + bSV_{L5}^{GPSi} + bant_{L5}^{GPSi})$$

$$b^{GALj} = \frac{f_{E1}^2}{f_{E1}^2 - f_{E5a}^2} (bsig_{E1}^{GALj} + bSV_{E1}^{GALj} + bant_{E1}^{GPSj}) + \frac{f_{E5a}^2}{f_{E5a}^2 - f_{E1}^2} (bsig_{E5a}^{GALj} + bSV_{E5a}^{GALj} + bant_{E5a}^{GALj})$$

NOMINAL BIAS DUE TO NOMINAL SIGNAL DEFORMATION

Nominal signal distortions are perturbations affecting the time domain waveform transmitted by the satellite as observed by the receiver. Alternatively, nominal signal deformations could be defined as perturbations affecting the correlation between the incoming signal and the locally generated replica in the receiver. These distortions affect L1, E1, L5 and E5a measurements independently as these 4 signals are different and because their respective tracking modules within the receiver are different. These nominal deformations affecting each individual L1, E1, L5, E5a measurement affect in turn the L1/L5 and E1/E5a iono-free measurements as per the L1/L5 and E1/E5a iono-free combination. These nominal deformations are assumed to affect only code pseudorange measurements. Indeed, it is assumed that nominal signal deformations induce a negligible error on phase measurements due to negligible prompt correlation loss. Therefore, the smoothed measurements are affected only through the perturbation of the iono-free code pseudorange measurements. Nominal signal distortions were modeled as the combination of digital distortions and analog distortions.

Nominal signal distortions were measured for example by Stanford University (SU) for all GPS satellites on L1 and L5 that could be observed at the time of measurement [Wong et al., 2010]. An average model for analog signal distortions, involving a specific spectrum shape inducing the average nominal time domain waveform shape based on the observations, was proposed in [Phelts et al., 2009]. In this reference, a limit for the oscillations in the amplitude/time domain for nominal versus deformed waveforms (evil waveforms) was also proposed. Among others, the observations of nominal deformations show that the maximum observed $\text{abs}(\Delta)$ for GPS L1 C/A is equal to 10 ns. From [Wong et al., 2010], we can also observe that only one L5 signal was observed, with $\Delta=4$ ns for the pilot L5 component and $\Delta=5$ ns for the L5 data component. These observations also show that nominal analog deformations are not 2nd order.

Nominal signal distortions for non observed GPS satellites are unknown, and nominal signal distortions for GALILEO E1 OS and E5a are unknown.

For this work, despite the observations made in [Wong et al., 2010], for this work, ENAC has chosen to model GPS nominal analog signal deformations for each SV as the result of a 2nd order filter with parameters at the limit of EWF parameters and varying for each PRN, and digital signal deformations are modeled for each SV as a time shift of the trailing or leading bit edge as per measurements available in the literature.

This is a tentative to use extreme nominal signal deformation with varying parameters for each PRN to analyze the performance of ARAIM in presence of nominal biases. Indeed, the upper bound on nominal signal deformations, and the worst-case dispersion of these deformations across the satellite constellation, are not defined in any standard.

So for GPS L1 C/A, ENAC used the best-case faulty EWF Threat Model B ($\Delta \approx 0$).

The best case Threat Model B digital deformation is around 0, so the digital deformations used for our model were taken as per the measurements made by Stanford University for each observed PRN.

For GPS L1 C/A, the best-case Threat Model B analog deformations are assumed to originate from a 2nd order filter with $F_d=17\text{MHz}$, $\sigma=0.8 \dots 8.8$ as a function of increasing PRN#. However, it is important to remember that nominal analog deformations are not 2nd order, but the choice of a 2nd order filter is assumed to reflect an extreme situation of these nominal analog deformations.

For GPS L1 C/A, as we can see in figures 1 and 2, $F_d=17\text{MHz}$ brings the lowest tracking biases for $BW < 24$, for any C_s within $0.01 \dots 0.5$ chip.

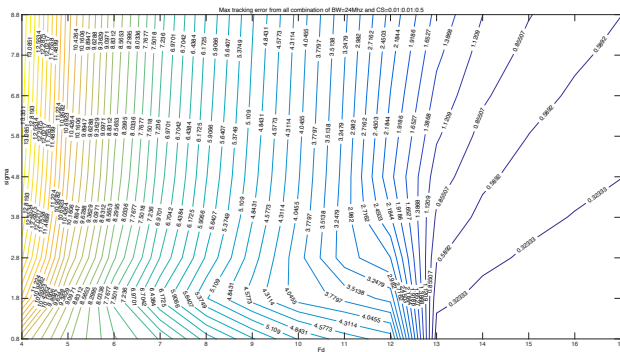


Figure 1: Maximum value of tracking bias for a GPS L1 C/A receiver with $BW=24$ MHz and chip spacing within $0.01 \dots 0.5$, as a function of F_d and σ .

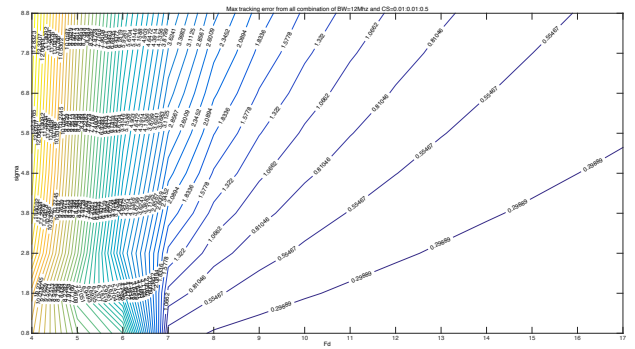


Figure 2: Maximum value of tracking bias for a GPS L1 C/A receiver with $BW=12$ MHz and chip spacing within $0.01 \dots 0.5$, as a function of F_d and σ .

As we can also see in these figures 1 and 2, $\sigma=0.8$ leads to the lowest tracking errors, but the nominal analog deformations observed by Stanford University have diverse values of the damping factor, and we need to create a strong diversity of the nominal bias across all satellites, so we chose to sample the $F_d=17\text{MHz}$ boundary: $\sigma=0.8 \dots 8.8$.

For GPS L5, ENAC also tried to use an extreme nominal deformation for this analysis derived as a lower bound of an EWF threat model. However, EWF threat model is not standardized yet for GPS L5. So ENAC proposes a faulty L5 EWF Threat Model B ($\Delta \approx 0$), where $\Delta = -0.6 \dots 0.6$ (L5 Chip), $F_d=1 \dots 24\text{MHz}$, $\sigma=0.8 \dots 8.8$. So, for GPS L5, ENAC used the best case faulty EWF Threat Model B ($\Delta \approx 0$) proposed above. The best case Threat Model B digital deformation is around 0, so the digital deformations were taken as per Stanford University measurements for each observed PRN. The best-case Threat Model B analog deformations were assumed to originate from a 2nd order filter with $F_d=24\text{MHz}$, $\sigma=0.8 \dots 8.8$ as a function of increasing PRN# in order to create a strong diversity of the nominal bias across all satellites.

However, it is unsure of how much this choice leads to an upper bound. Indeed, the choice to model limit nominal analog deformations as a 2nd order filter with parameter values equal to limit EWF threat model B brings a limit for 2nd order nominal deformations, but it may be possible that other limit nominal deformations occur that lead to worse ARAIM performance. Other options could have been chosen, such as using the limit 2nd order deformed model expressed in the amplitude/time domain, where the limits are taken from [Phelts et al., 2009], and use another model for the dispersion of the nominal biases across all the satellites. The use of real observed nominal analog deformation with their natural dispersion across satellites is another option that is necessary to consider, as in [PHELTS et al., 2014a].

From these assumptions, a table has been built by ENAC to model the code pseudorange biases induced by nominal signal deformations for GPS L1 C/A signal component.

ARAIM user receiver code tracking errors induced by these limit GPS L1 C/A nominal signal deformations were then computed for E-L discriminator, and for Chip Spacing (Cs), bandwidth (BW) within a BW-Cs region defined later in this paper, considering first the latest BW-Cs region proposed by Stanford University at RTCA, and a BW-Cs region within which the ranging error is limited. ARAIM tracking error due to nominal signal deformation was not computed for double delta discriminator as SU proposal to RTCA is to remove it from the set of authorized configurations.

Also, the induced ranging errors were computed assuming a combined RF/IF filter modeled as a butterworth (order 6) filter with differential group delay of 150 ns, as per the ICAO SARPs requirements for $BW \geq 7$ MHz.

Indeed, the new (Cs, BW) region proposed by SU at RTCA for BPSK [PHELTS et al., 2014b] can be summarized as follows:

- Only allow early minus late correlator (terminal area not considered)
- L1 C/A
 - BW between 12 and 24 MHz
 - Cs between 0.08 and 0.12
 - Group delay < 150 nsec (including antenna)
- L5/E5A
 - BW = tight region around 24 MHz
 - Cs = tight region around 1 chip
 - Exact region TBD
 - Group delay < 150 nsec (including antenna)

Reference configuration is for GPS L1 C/A BW=24 MHz – Cs=0.1, and for GPS L5/GALILEO E5a BW=24 MHz – Cs=1.

Based on these assumptions, the nominal biases due to nominal signal deformation are shown in the following figures.

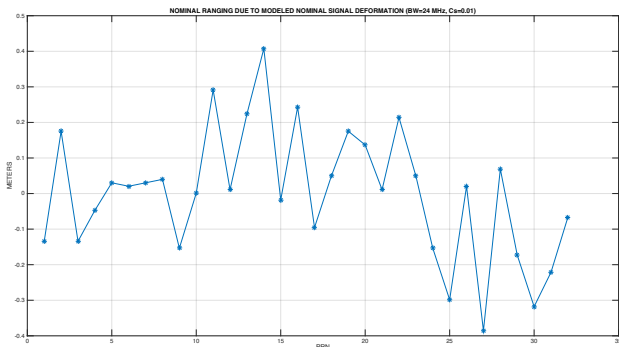


Figure 3: Nominal GPS L1 C/A bias due to modeled nominal signal deformation for each considered GPS, for BW=24MHz, Cs=0.1 chip (same table used for GALILEO E1 OS).

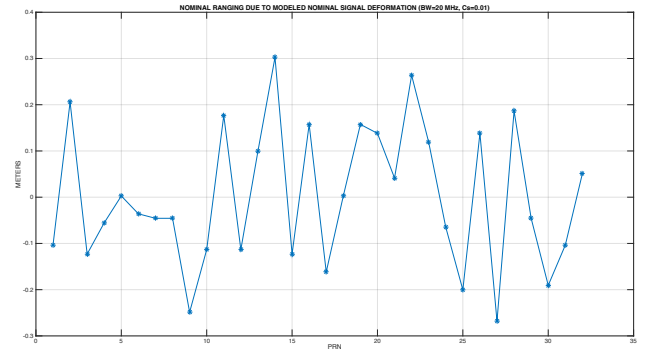


Figure 4: Nominal GPS L1 C/A bias due to modeled nominal signal deformation for each considered GPS, for BW=20MHz, Cs=0.1 chip (same table used for GALILEO E1 OS).

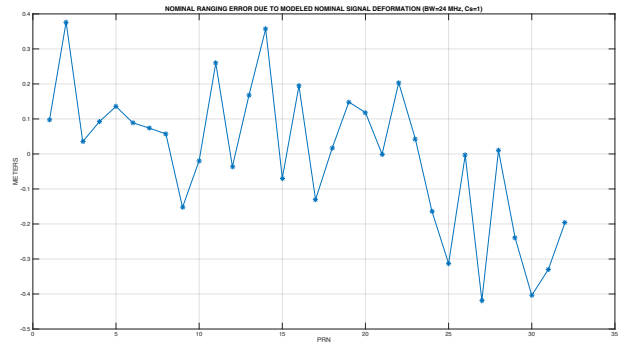


Figure 5: Nominal GPS L5 bias due to modeled nominal signal deformation for each considered GPS, for BW=24MHz, Cs=1 chip (same table used for GALILEO E5a).

Other pairs of (BW, Cs) were tested in order to evaluate the sensitivity of the results to that parameter and to get results for other communities of users with different receiver designs.

The tracking errors induced by these extreme nominal signal deformations were computed.

It appears interesting to determine the impact of deviations of the receiver configuration from the receiver characteristics as proposed by Stanford University.

Indeed, we can define an ARAIM user Rx BW, Cs area for a maximum deviation of the limit nominal bias w.r.t the reference bias, so that this value is lower than a threshold (ex: 0.1m).

So we can for example compute

$$\max_i |b^i(BW, Cs) - b^i(BW_{ref}, Cs_{ref})|$$

across all SVs_i, affected by their extreme nominal deformation for all BW and Cs within a specific region.

This may provide an additional criterion for allowed receiver configurations (BW, Cs).

Several factors impact this value:

- Model for limit nominal biases due to signal deformation

- BW_{ref} and Cs_{ref}
- Type of RF/IF filter used for reference (magnitude, grp delay)
- Type of RF/IF filter for ARAIM user Rx (magnitude, group delay)

We first consider that the user Rx has an RF/IF filter modeled as a 6th order butterworth filter with a differential group delay forced to be equal to 150ns. But we also have to consider that the reference RF/IF filter may be different from the user RF/IF filter. Indeed, the differential group delay has an important impact.

The specification for the RF/IF filter group delay is proposed to be kept such that $\Delta gd < 150$ ns including the antenna differential group delay.

Then, we also considered an RF/IF filter modeled as a 6th order butterworth, or a 6th order chebychev with natural group delay. We also considered an RF/IF filter modeled as a SAW filter (diff group delay=0 in the 3dB BW).

Based on the assumptions presented above, we therefore determined the variations on the extreme nominal bias induced by variations on the chip spacing or on the bandwidth of the user receiver.

Figure 6 shows the contour plot of this relative difference between the nominal GPS L1 C/A bias induced by each GPS SVs affecting a user coping exactly with the proposed characteristics $BW_{ref}=24$ MHz, $Cs_{ref}=0.1$ and a user having different BW, Cs than this proposition.

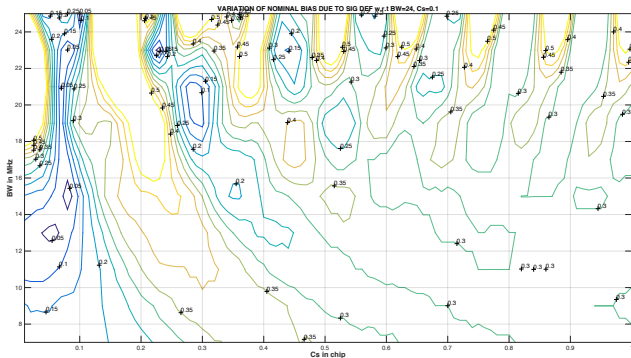


Figure 6: Maximum value across all SVs of difference in nominal tracking bias for each SV as a function of BW, Cs w.r.t. nominal tracking bias for $BW_{ref}=24$ MHz, $Cs_{ref}=0.1$ (Δ as per SU measurements, $F_d=17$ MHz, $\sigma=0.8 \dots 8.8$, Ref and user RF/IF filter: butter6, $\Delta gd=150$ ns).

As we can see in figure 6, a very narrow area with a max variation of 10 cm appears in the upper left corner, including narrow Cs with a low BW in the lower left corner. This area is shown in figure 7 below.

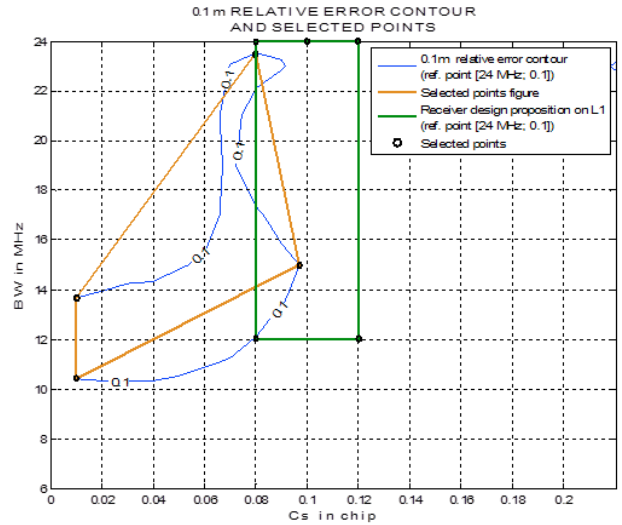


Figure 7: Zoom on maximum value across all SVs of difference in nominal tracking bias for each SV as a function of BW, Cs w.r.t. nominal tracking bias for $BW_{ref}=24$ MHz, $Cs_{ref}=0.1$ (Δ as per SU measurements, $F_d=17$ MHz, $\sigma=0.8 \dots 8.8$, Ref and user RF/IF filter: butter6, $\Delta gd=150$ ns).

If we consider this 10 cm max deviation area, key points to be tested are then listed in the table below:

[24 MHz;0.12]
[24 MHz;0.08]
[12 MHz;0.08]
[12 MHz;0.12]
[24 MHz;0,1]
[20 MHz;0,1]
[23.5MHz;0.08]
[15MHz;0.0969]
[10,5MHz;0.0101]
[13.7MHz;0.0104]

Table 1: List of BW, Cs points considered for further testing ($BW_{ref}=24$ MHz, $Cs_{ref}=0.1$).

Figure 8 shows the contour plot of this relative difference between the nominal GPS L1 C/A bias induced by each GPS SVs affecting a user coping exactly with the proposed characteristics $BW_{ref}=20$ MHz, $Cs_{ref}=0.1$ and a user having different BW, Cs than this proposition.

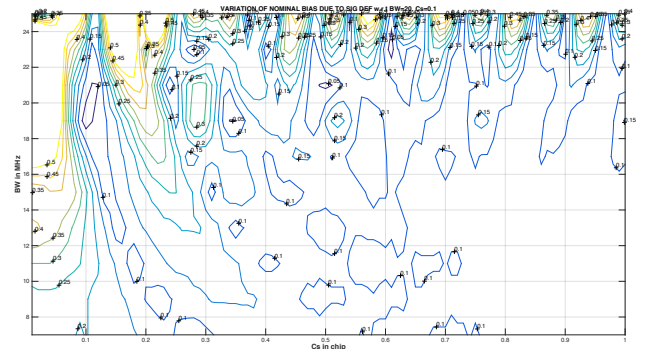


Figure 8: Maximum value across all SVs of difference in nominal tracking bias for each SV as a function of BW, Cs w.r.t. nominal tracking bias for BWref=20 MHz, Csref=0.1 (Δ as per SU measurements, Fd=17MHz, $\sigma=0.8 \dots 8.8$, Ref and user: butter6, $\Delta_{gd}=150$ ns).

As we can see, the 10 cm max error contour now fits better the 1/BW hyperbola, and a large plateau appears for all BW<20 and Cs>0.3.

A zoom on this figure is shown in figure 9 below.

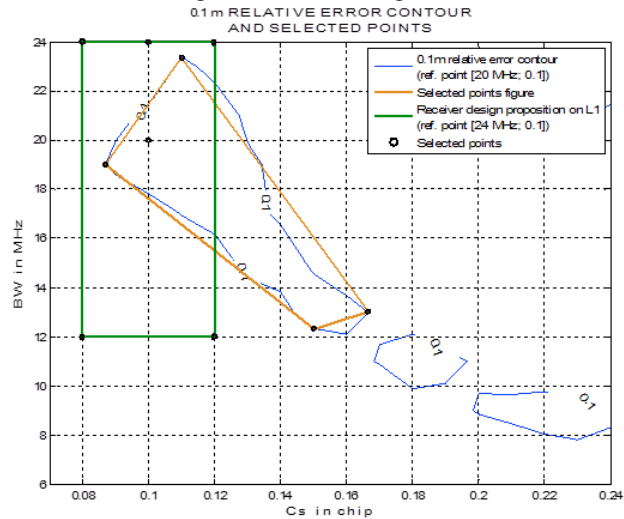


Figure 9: Zoom on maximum value across all SVs of difference in nominal tracking bias for each SV as a function of BW, Cs w.r.t. nominal tracking bias for BWref=20 MHz, Csref=0.1 (Δ as per SU measurements, Fd=17MHz, $\sigma=0.8 \dots 8.8$, Ref and user RF/IF filter: butter6, $\Delta_{gd}=150$ ns).

If we consider this 10 cm max deviation area, key points to be tested are then listed in the table below:

[24 MHz;0.12]
[24 MHz;0.08]
[12 MHz;0.08]
[12 MHz;0.12]
[24 MHz;0.1]
[20 MHz;0.1]
[23.4MHz;0.11]
[19MHz;0.0869]
[12.3MHz;0.151]
[13MHz;0.167]

Table 2: List of BW, Cs points considered for further testing (BWref=20MHz, Csref=0.1).

One possible criterion to adopt a specific BW, Cs configuration could then be to adopt a specific tolerance on the limit nominal bias induced by each SV. If a tolerance of 10 cm is adopted, it would therefore be allowed the BW, Cs points within the contour drawn at 0.1 m in the figure above.

However, the possible criterion to be adopted depends on the overall ARAIM system architecture, and its global performance for the user.

This aspect will be covered in the last part of this paper.

Concerning L5, the maximum variations were found to be limited to 0.1m for a large range of BW and Cs values, as shown in the figure below.

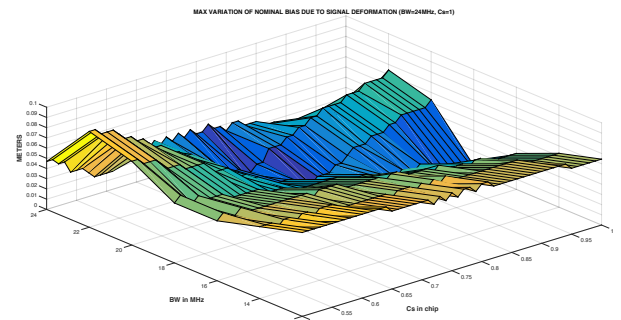


Figure 10: Maximum value across all SVs of difference in nominal tracking bias for each SV as a function of BW, Cs w.r.t. nominal tracking bias for BWref=24 MHz, Csref=1 (Δ as per SU measurements, Fd=24MHz, $\sigma=0.8 \dots 8.8$, Ref and user RF/IF filter: butter6, $\Delta_{gd}=150$ ns).

As a conclusion, for GPS L5 and GALILEO E5a, the configuration was set to fixed for the reference and for the ARAIM user to be equal to BW=24 MHz and Cs=1 chip.

NOMINAL BIAS DUE TO USER ANTENNA GROUP DELAY VARIATION

ARAIM user antenna induces a group delay variation according to the angle of arrival with respect to the center of measurement, from which all signals at the same carrier frequency and bandwidth have the same path length to the signal processing module. ENAC had built a table for GPS L1 C/A range error from results of GPS L1 EM modelling in [MURPHY et al., 2007], illustrated in figure 11 below.

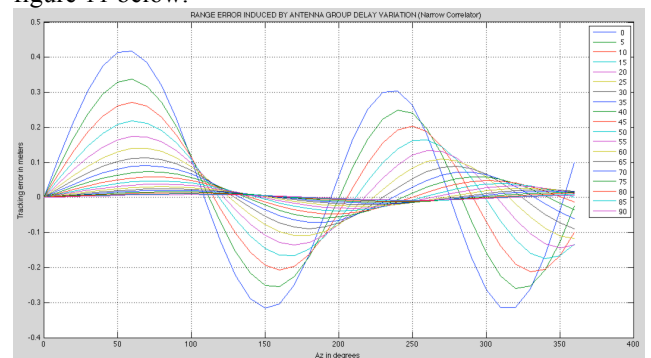


Figure 11: Tracking error induced by modeled antenna group delay variation as a function of Az and El for GPS L1 C/A.

The same table had been used for GPS L5, GALILEO E1 OS, GALILEO E5a.

However, this model does not take into account the influence of the aircraft structure. It would also be of interest to model the variation of the user antenna group delay for a dual frequency L1/L5 civil aviation aircraft antenna.

Therefore, ENAC has launched a study to determine the value of this group delay for a dual frequency L1/L5 civil aviation aircraft antenna.

Figure 12 shows an illustration of the modeled antenna.

It is to be noted that this simulated antenna does not fully comply with the gain requirements expressed in the EUROCAE draft antenna MOPS [EUROCAE, 2013]. Indeed, as shown in figures 9 and 10, its gain at low elevation is not sufficiently large as it should be larger than -11 dB on the horizon. It is thought that this deviation from the specification does not influence the final result.

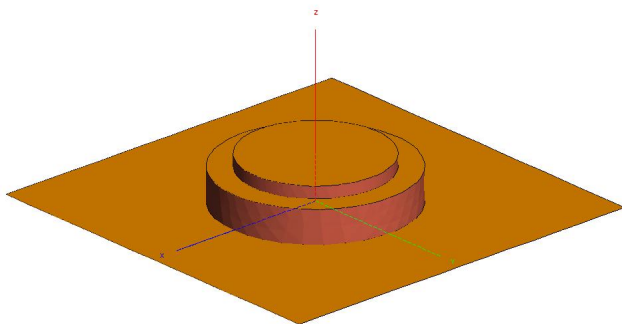


Figure 12: Illustration of modeled circular L1/L5 stacked patch antenna.

This antenna is modeled as a circular stacked patch antenna with 4 feedings. It is a dual band L1E1 and L5E5a.

Its performance was simulated with Feko software (<https://www.feko.info/>).

The free space L1 gain pattern of this antenna is as shown in the next figure:

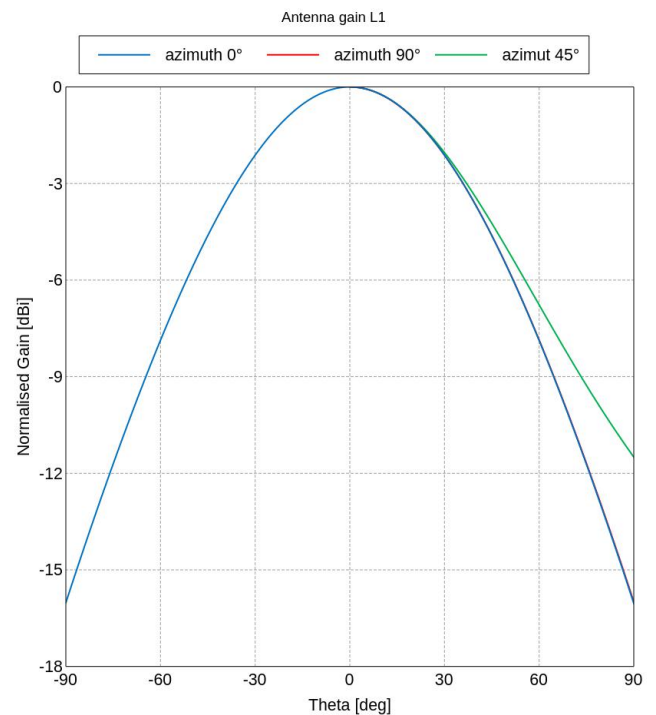


Figure 13: Illustration of L1 free space gain pattern of modeled circular L1/L5 stacked patch antenna.

The free space L5 gain pattern of this antenna is as shown in the next figure:

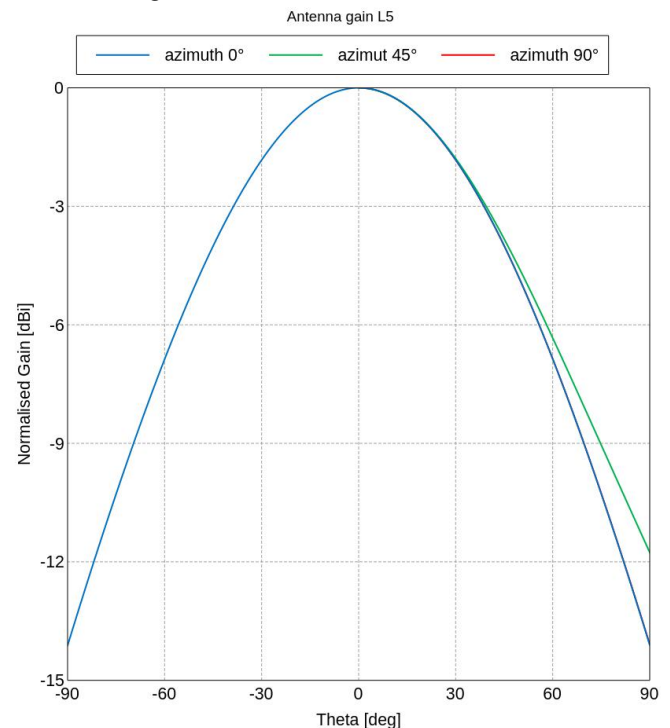


Figure 14: Illustration of L5 free space gain pattern of modeled circular L1/L5 stacked patch antenna.

Two types of simulations were run:

- simulation of the antenna in free-space
- simulations of the antenna plus the main scattering part of an A380 aircraft (tail, wings, fuselage)

The model of the antenna mounted on the fuselage of an A380 aircraft is illustrated in figure 14 below, as well as the definition of the elevation and azimuth angles used for antenna characterization.

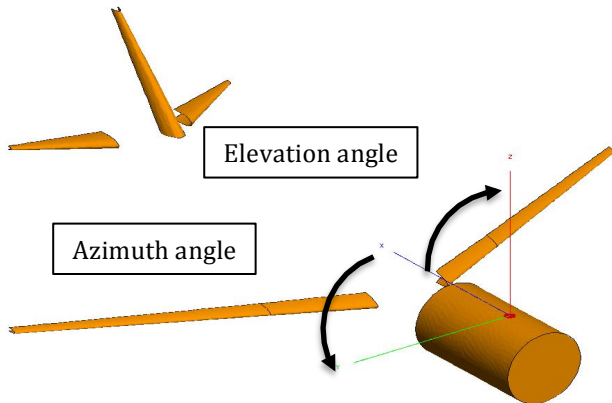


Figure 15: Illustration of modeled circular L1/L5 stacked patch antenna mounted on fuselage of A380 aircraft.

As we can see in this figure 14, the main body of the fuselage itself is not considered, as it does not have an electromagnetic influence.

Using this model, the radiated electromagnetic fields were simulated, and the group delay was derived as:

$$\tau = -\frac{1}{2\pi} \frac{d\varphi}{df}$$

where φ is the phase of the radiation pattern in co-polarization.

The L1 gain pattern of this antenna mounted on the A380 aircraft model is as shown in the next figure:

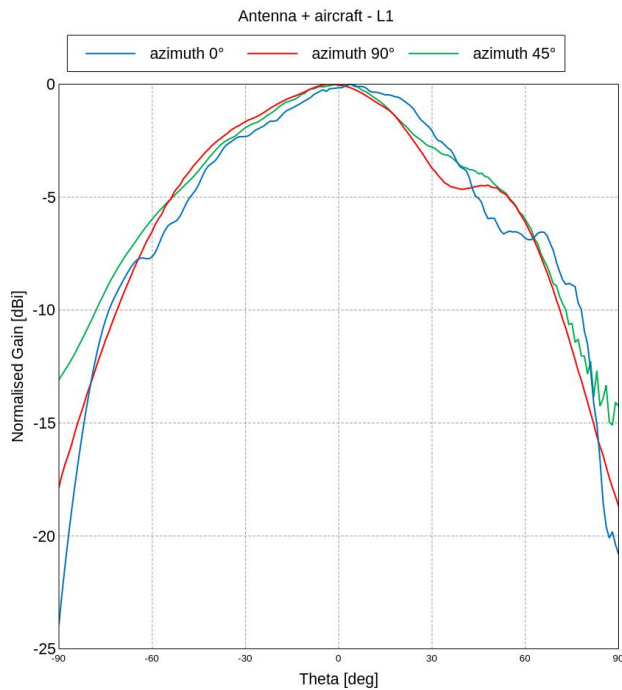


Figure 16: Illustration of L1 gain pattern of modeled circular L1/L5 stacked patch antenna mounted on fuselage of A380 aircraft.

The L5 gain pattern of this antenna mounted on the A380 aircraft model is as shown in the next figure:

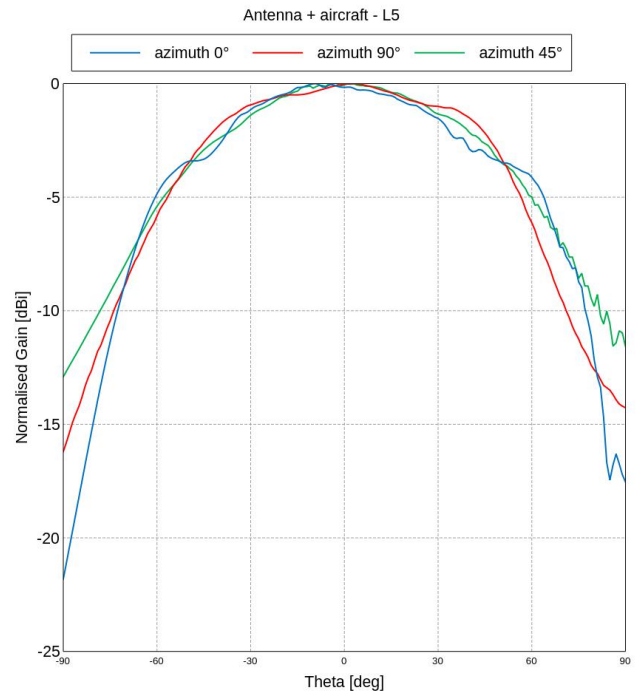


Figure 17: Illustration of L5 gain pattern of modeled circular L1/L5 stacked patch antenna mounted on fuselage of A380 aircraft.

The variation of the group delay as a function of the direction of the incident field has been computed. The antenna group delay is referenced w.r.t mean group delay at 5° elevation across all azimuth angles.

The 3D plot of the observed group delay on L1 of the antenna in free space is shown in the next figure.

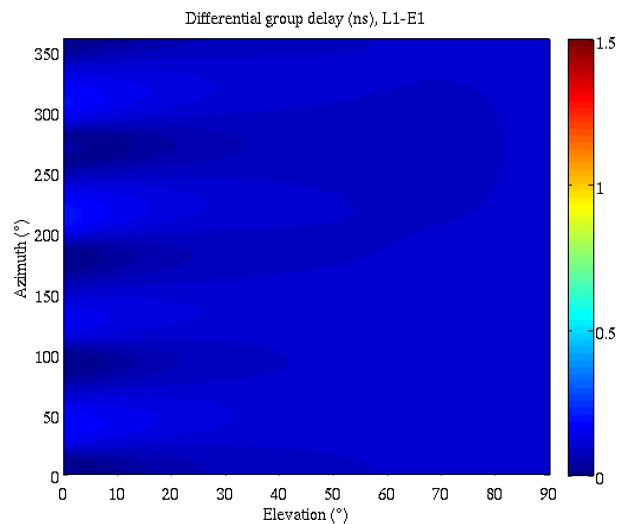


Figure 18: Illustration of L1 group delay of modeled circular L1/L5 stacked patch antenna in free space, as a function of azimuth & elevation angles of incident field .

The complete plot of the group delay of this antenna in free space on L1 as a function of the elevation and azimuth angles is shown in figure 19.

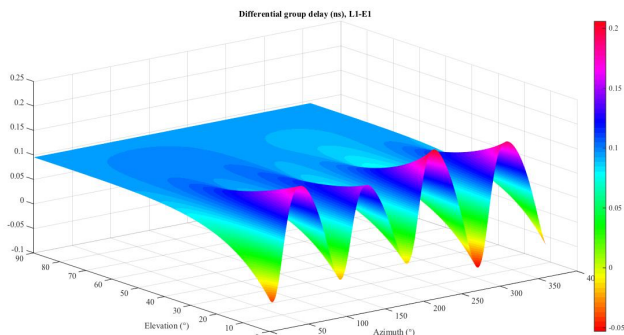


Figure 19: Illustration of L1 group delay of modeled circular L1/L5 stacked patch antenna in free space, as a function of angles of elevation and azimuth of incident field.

The complete plot of the group delay of this antenna in free space on L1 as a function of the elevation angle is shown in figure 20.

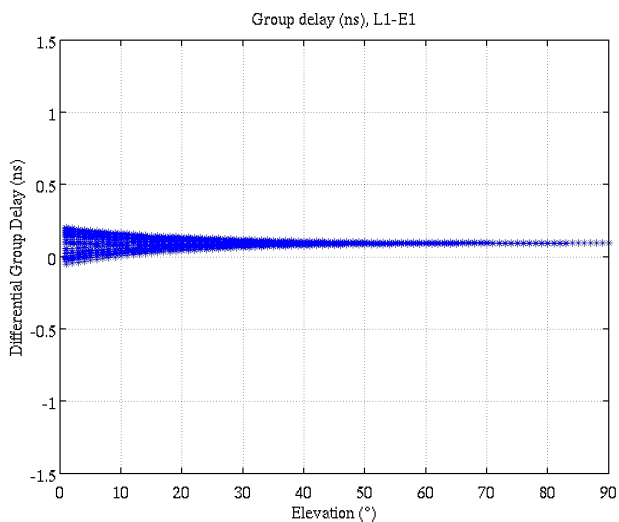


Figure 20: Illustration of L1 group delay of modeled circular L1/L5 stacked patch antenna in free space, as a function of angle of elevation of incident field.

The complete plot of the group delay of this antenna in free space on L1 as a function of the azimuth angle is shown in the next figure.

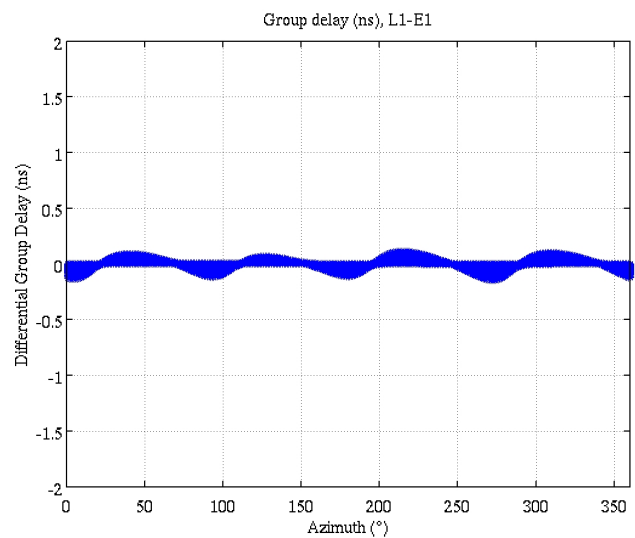


Figure 21: Illustration of L1 group delay of modeled circular L1/L5 stacked patch antenna in free space, as a function of angle of azimuth of incident field.

As we can see, this L1 group delay has a maximum variation of +/-0.2 ns or equivalently +/-6 cm across all elevation and azimuth angles.

This has to be considered jointly with the draft EUROCAE L1/L5 antenna MOPS requirement that states that the maximum $\Delta g_d < 25$ ns on each band, and the maximum $\Delta g_d < 3$ ns as a function of Az, El [EUROCAE, 2013].

However, considering this user antenna as in free space only may not reflect the reality of the group delay variation affecting the pseudorange measurements made by the user receiver. A tentative was made to evaluate the impact of the aircraft structure on the variation of the group delay affecting the final pseudorange measurement made by the receiver. This new group delay can be seen as the group delay of a narrow band signal around the carrier frequency tracked by the receiver after considering the impact of the aircraft structure plus the antenna. This may therefore reflect the tracking error made by a narrow band receiver tracking this narrow band signal arriving with a static specific angle of arrival due to multipath created by the aircraft structure as seen by this antenna. This does not reflect the actual GNSS situation, as the GNSS signal is wideband and the direction of arrival changes with time. However, this situation may be closer to reality than considering the antenna in free space.

The 3D plot of the observed group delay on L1 of the antenna mounted on an A380 aircraft is shown in the next figure.

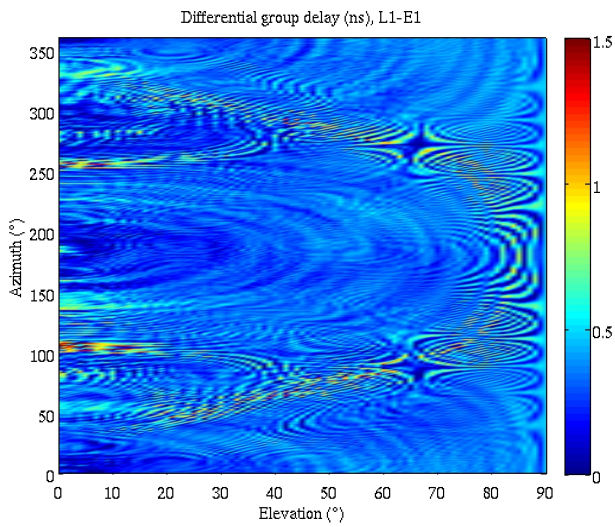


Figure 22: Illustration of L1 group delay of modeled circular L1/L5 stacked patch antenna mounted on fuselage of A380 aircraft.

The complete plot of the group delay of this antenna mounted on A380 aircraft on L1 is shown in figure 23.

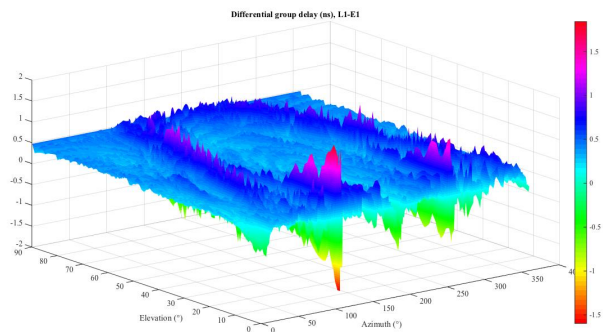


Figure 23: Illustration of L1 group delay of modeled circular L1/L5 stacked patch antenna in free space, as a function of angles of elevation and azimuth of incident field.

The complete plot of the group delay of this antenna mounted on A380 aircraft on L1 is shown in the next figure.

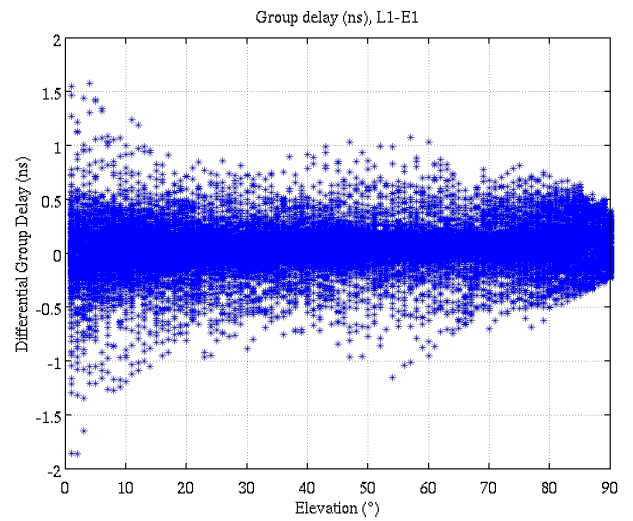


Figure 24: Illustration of L1 group delay of modeled circular L1/L5 stacked patch antenna in free space, as a function of angle of elevation of incident field.

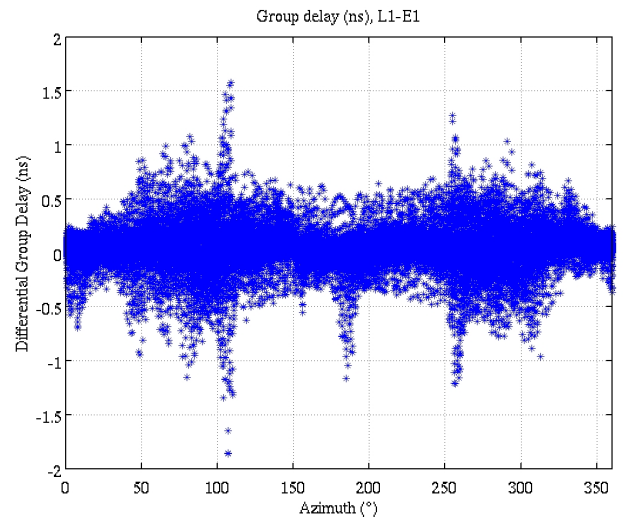


Figure 25: Illustration of L1 group delay of modeled circular L1/L5 stacked patch antenna in free space, as a function of angle of elevation of incident field.

As we can see, this L1 group delay has a maximum variation of ± 2 ns or equivalently ± 60 cm across all elevation and azimuth angles.

The 3D plot of the observed group delay on L5 of the antenna in free space is shown in the next figure.

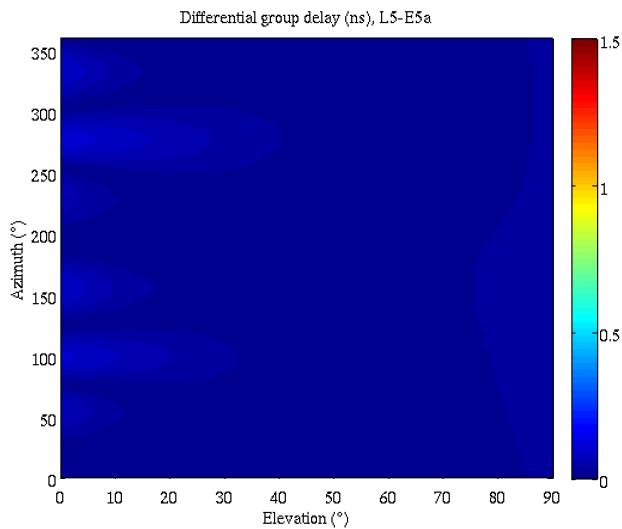


Figure 26: Illustration of L5 group delay of modeled circular L1/L5 stacked patch antenna in free space, as a function of azimuth & elevation angles of incident field.

The complete plot of the group delay of this antenna in free space on L5 as a function of the elevation angle is shown in the next figure.

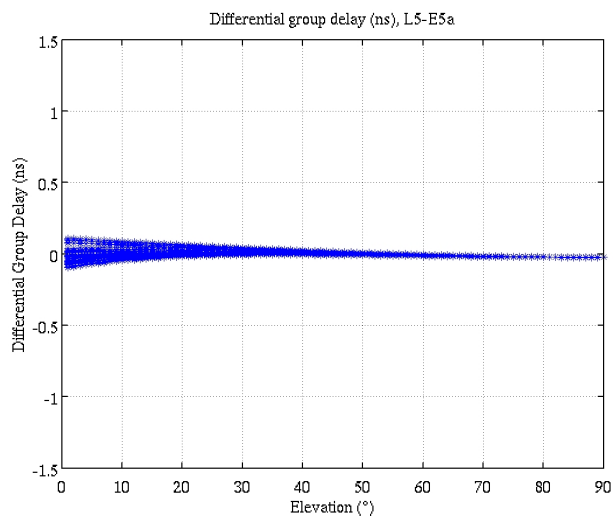


Figure 27: Illustration of L5 group delay of modeled circular L1/L5 stacked patch antenna in free space, as a function of angle of elevation of incident field.

The complete plot of the group delay of this antenna in free space on L5 as a function of the azimuth angle is shown in the next figure.

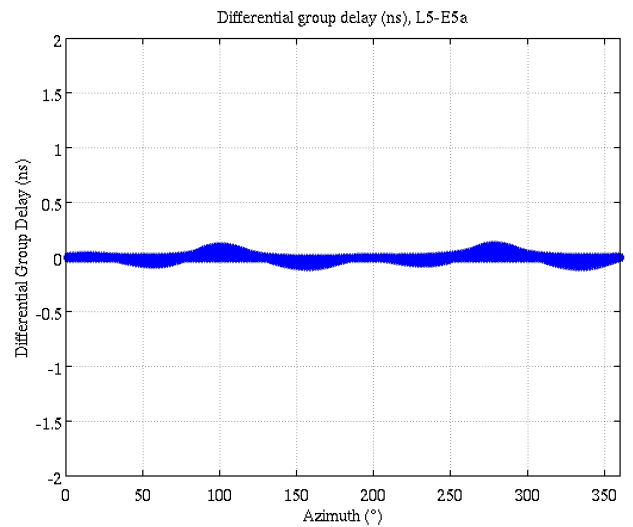


Figure 28: Illustration of L5 group delay of modeled circular L1/L5 stacked patch antenna in free space, as a function of angle of azimuth of incident field.

As we can see, this L5 group delay has a maximum variation of ± 0.1 ns or equivalently ± 3 cm across all elevation and azimuth angles.

The 3D plot of the observed group delay on L5 of the antenna mounted on an A380 aircraft is shown in the next figure.

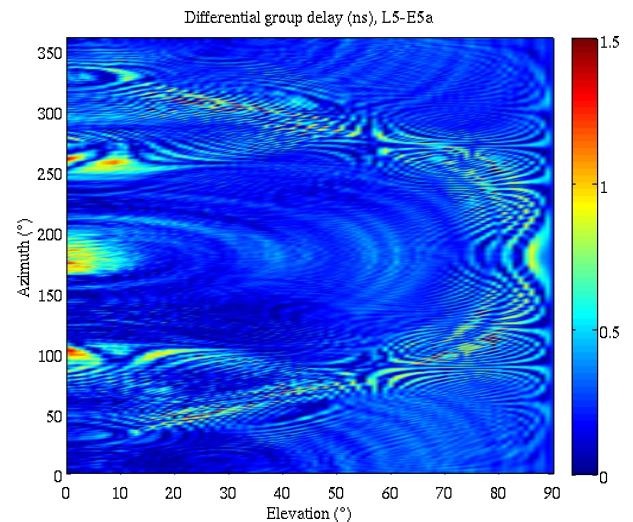


Figure 29: Illustration of L5 group delay of modeled circular L1/L5 stacked patch antenna mounted on fuselage of A380 aircraft.

The complete plot of the group delay of this antenna mounted on A380 aircraft on L5 as a function of the elevation angle is shown in the next figure.

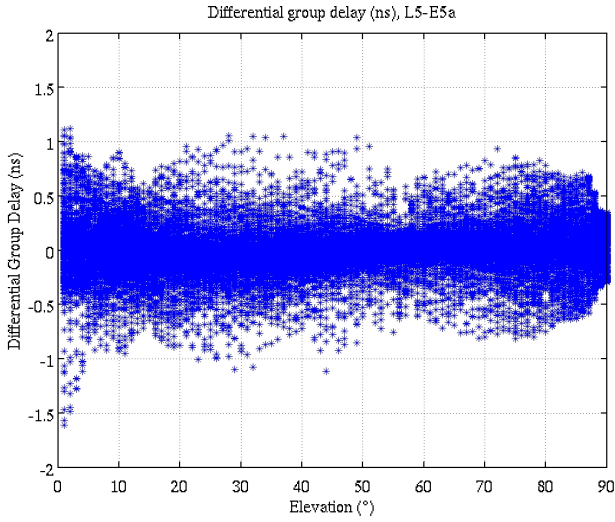


Figure 30: Illustration of L5 group delay of modeled circular L1/L5 stacked patch antenna in free space, as a function of angle of elevation of incident field.

The complete plot of the group delay of this antenna mounted on A380 aircraft on L5 as a function of the elevation angle is shown in the next figure.

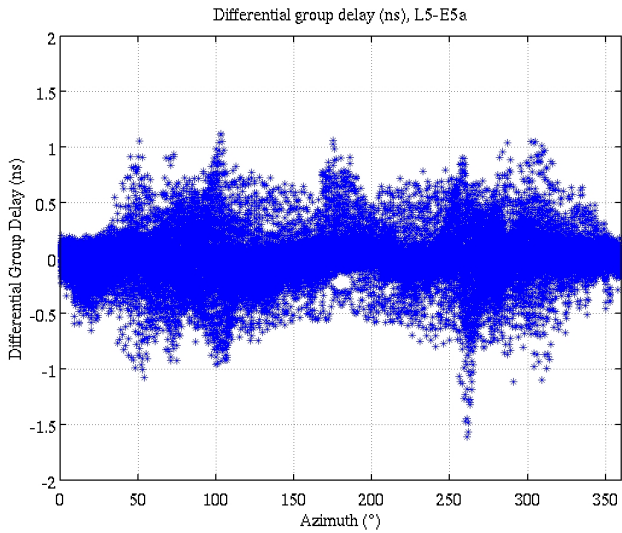


Figure 31: Illustration of L5 group delay of modeled circular L1/L5 stacked patch antenna in free space, as a function of angle of elevation of incident field.

As we can see, this L5 group delay of the L1/L5 antenna mounted on the aircraft has a maximum variation of +/-2 ns or equivalently +/- 60 cm across all elevation and azimuth angles.

The question of the most appropriate technique for protection of the ARAIM user against the impact of the ranging error induced by the user antenna group delay then arises. Several options exist, that include the consideration of the worst-case conspiring situation of these ranging errors, or the consideration of this ranging error as a random variable at each epoch.

On one hand, the ARAIM user antenna bias for each SV may be very stable along the duration of each single approach made by an aircraft, but its exact time domain variation during the approach is not clearly known. Indeed, smoothed user antenna group delay may be constant for high elevation SVs as shown in the previous plots, but may also vary during approach for low elevation SVs as aircraft attitude varies by a few degrees. On the other hand, the ARAIM user antenna biases vary across all situations faced by ARAIM users and are difficult to predict (these biases depend on antenna, runway orientation, SV angle of arrival, aircraft attitude, aircraft).

We made the choice in this paper to assume that these biases are a low pass random process and are included into the multipath budget $\sigma_{mult_IF} = \sqrt{\gamma_1^2 + \gamma_2^2} (0.13 + 0.53e^{-\theta/10})$ m.

This assumption will need further validation.

In this paper, we also provide a contribution to the analysis of the time domain variation of the ARAIM user antenna bias.

We considered real attitude angles observed during one approach of an A380 at Toulouse Blagnac airport. We then considered each possible GNSS signal angle of arrival on a grid 0...90° in elevation and 0...359° in azimuth. For each of these signals, we assumed that the L1/L5 ionofree measurement made by the ARAIM receiver is affected by a ranging error equal to the group delay plotted in the previous figures. 400 seconds before crossing the FAF, we then initiated a 100s time constant smoothing filter replicating a possible 100s code-carrier smoothing filter applied on this measurement. Due to aircraft attitude variation during the approach, any signal viewed by the aircraft antenna with an elevation lower than 5° is dropped and not considered in final statistics. This analysis has been done by taking into account the impact of the aircraft fuselage.

Figure 32 shows a projection of the estimated average value of the smoothed L1/L5 ionofree group delay as a function of the elevation angle in meters.

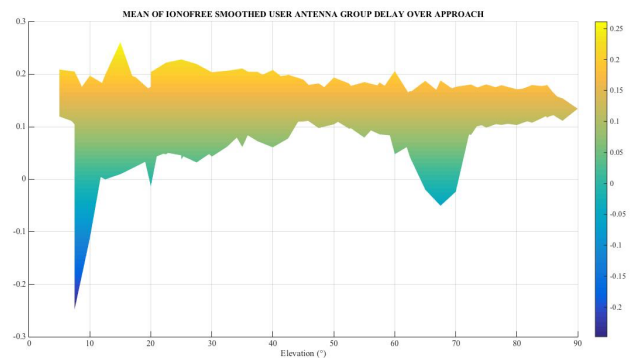


Figure 32: Illustration of estimated mean of L1/L5 ionofree smoothed group delay of modeled circular L1/L5

stacked patch antenna mounted on aircraft, as a function of angle of elevation of incident field.

As we can see, the average value is approximately constantly equal to 15 cm for elevations larger than 45° and for a large range of azimuth angles, but has larger variations when the elevation angle is lower.

Figure 33 shows the estimated standard deviation of the smoothed L1/L5 ionofree group delay, as well as $\sigma_{mult_IF} = \sqrt{\gamma_1^2 + \gamma_2^2} (0.13 + 0.53e^{-\theta/10})$ m.

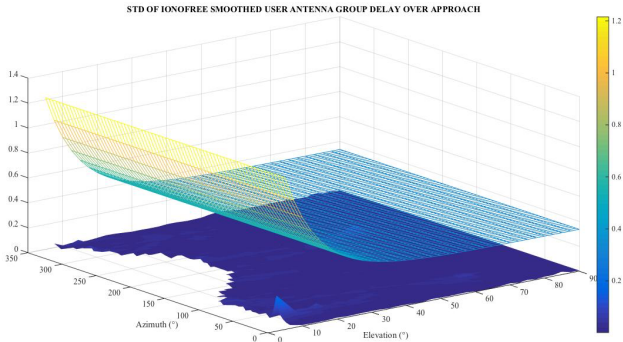


Figure 33: Illustration of estimated standard deviation of L1/L5 ionofree smoothed group delay of modeled circular L1/L5 stacked patch antenna mounted on aircraft, as a function of angle of azimuth and elevation of incident field.

As we can see, this estimated standard deviation is lower than 10 cm for elevations larger than 30°, and its maximum value is 22 cm at 5° elevation. The low value of the standard deviation at high elevation angles indicates that this smoothed group delay is very stable along the approach, while having a stable mean value around 15 cm as seen previously, for signals in these directions of arrival. Also, we can see that this standard deviation is very much lower than the assumed standard deviation of the multipath error.

As this error can have quite a signification mean value, we also evaluated the RMS of this smoothed ionofree group delay, which is plotted in figure 34.

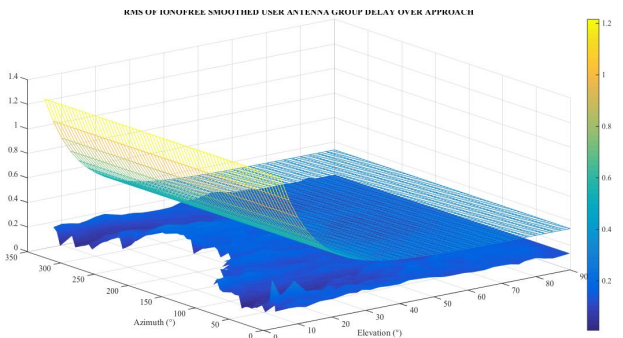


Figure 34: Illustration of estimated RMS of L1/L5 ionofree smoothed group delay of modeled circular L1/L5

stacked patch antenna mounted on aircraft, as a function of angle of azimuth and elevation of incident field.

As we can see as well, the RMS of this ionofree group delay has a maximum value of 33 cm at 5°, and is always lower than the assumed standard deviation of the ionofree multipath error.

Therefore, from this evaluation with our models, it seems reasonable that this error is not considered as a nominal bias, but rather as a random variable at each epoch, having a distribution that is partly taken into account in the Gaussian distribution overbounding the 100s smoothed multipath error with standard deviation $\sigma_{mult} = 0.13 + 0.53e^{-\theta/10}$ m.

However, this is an initial contribution to this analysis, and this assumption needs to be further validated.

NOMINAL BIAS DUE TO SV ANTENNA GROUP DELAY VARIATION

Another slowly varying error could be taken into account in the set of the nominal biases, which is the bias due to the variation of the SV antenna group delay as a function of the nadir angle. Indeed, it is believed that this slowly varying error is not fully reflected in the URE.

ENAC built a table for GPS L1 measurements for all GPS SVs analyzed in [HAINES et al., 2012], as shown in figure 35. Indeed, [HAINES et al., 2012] have estimated the group delay variation as a function of the SV nadir angle from P1/P2 iono-free measurements.

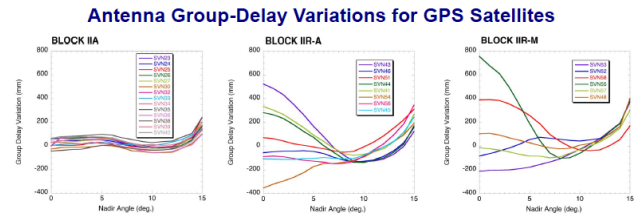


Figure 35: Illustration of variation of SV antenna group delay variation as a function of nadir angle [HAINES et al., 2012].

We assume that this estimated group delay variation is equal to a ranging bias $bSV_{L1/L2}^{GPSi}$ on the P1/P2 ionofree modeled as

$$bSV_{L1/L2}^{GPSi} = \frac{f_{L1}^2}{f_{L1}^2 - f_{L2}^2} bSV_{L1}^{GPSi} + \frac{f_{L2}^2}{f_{L2}^2 - f_{L1}^2} bSV_{L2}^{GPSi}$$

with

$$\frac{f_{L1}^2}{f_{L1}^2 - f_{L2}^2} \approx 2.546$$

$$\frac{f_{L2}^2}{f_{L2}^2 - f_{L1}^2} \approx -1.546$$

Assuming that each bSV_{L1}^{GPSi} and bSV_{L2}^{GPSi} is random with a decreasing distribution around 0, we assume that there is a large probability that $|bSV_{L1/L5}^{GPSi}| < |bSV_{L1/L2}^{GPSi}|$ and

$|bSV_{E1/E5a}^{GALj}| < |bSV_{L1/L2}^{GPSj}|$. For the simulations, we assume therefore $bSV_{L1/L5}^{GPSi} = bSV_{L1/L2}^{GPSi}$ and $bSV_{E1/E5a}^{GALj} = bSV_{L1/L2}^{GPSj}$.

ENAC built a similar table for GPS L1, GPS L5, GALILEO E1, GALILEO E5a SVs from GPS L1 observations in [HAINES et al., 2008].

This error has a long-term variation during a CAT-I approach, that could even be predicted. It is therefore felt appropriate to consider it as a nominal bias. For a different consideration, it remains also to be known in which existing error term this error could be fit (URE or σ_{mult}).

MODEL OF NOMINAL BIAS

We will finally use the final model for nominal biases:

$$b^{GPSi} = bSV_{L1/L5}^{GPSi} + \frac{f_{L1}^2}{f_{L1}^2 - f_{L5}^2} bsig_{L1}^{GPSi} + \frac{f_{L5}^2}{f_{L5}^2 - f_{L1}^2} bsig_{L5}^{GPSi}$$

$$b^{GALj} = bSV_{E1/E5a}^{GALj} + \frac{f_{E1}^2}{f_{E1}^2 - f_{E5a}^2} bsig_{E1}^{GALj} + \frac{f_{E5a}^2}{f_{E5a}^2 - f_{E1}^2} bsig_{E5a}^{GALj}$$

From the previous evaluations, the bias on the single frequency measurements due to nominal signal deformation has a max variation range of +/- 40 cm around the average value for all 32 SVs and the bias on iono-free measurements due to SV antenna group delay variation as a function of nadir angle has a variation range of +/- 50 cm around the average value for all 32 SVs.

Finally, if all two components are considered, the overall maximum variation range of the iono-free bias is approximately +/- 2 m around the average value obtained for all 32 SVs.

IMPACT ON ARAIM USER PERFORMANCE

The impact of nominal biases on the vertical position error can be modeled as:

$$VPE_{nb} = \sum_{i=1}^{NGPS} S_3^i b^{GPSi} + \sum_{j=NGPS+1}^N S_3^j b^{GALj-NGPS}$$

The nominal biases may also impact the integrity monitoring performance. Indeed, the nominal biases affect the iono-free pseudorange measurements used for positioning, thus affect the ARAIM algorithm test criteria for fault-detection and exclusion, although the impact of these biases is only partially taken into account through the URE in the detection threshold.

Nevertheless, the presence of these biases is taken into account in the computation of the protection levels by using the input ISM B_{nom} parameter. In particular, the VPL is calculated such that [EU-US, 2012].

$$2Q \left(\frac{VPL - b_3^{(0)}}{\sigma_3^{(0)}} \right) + \sum_{k=1}^{N_{faults}} P_{fault,k} Q \left(\frac{VPL - T_{k,3} - b_3^{(k)}}{\sigma_3^{(k)}} \right) = PHMI_{vert} - P_{sat,not\ monitored} - P_{const,not\ monitored}$$

The VPL terms bounding VPE_{nb} are the vertical position error bounds $b_3^{(k)}$:

$$b_3^{(k)} = \sum_{i=1}^{NGPS} |S_{3,i}^{(k)}| B_{nom,i}^{GPS} + \sum_{j=NGPS+1}^N |S_{3,j}^{(k)}| B_{nom,j-NGPS}^{GAL}$$

We see therefore here the dependence between the $B_{nom,i}$ and the VPL.

The terms B_{nom} should be bounds on nominal biases such that $b^{(k)}$ are proper bounds of the impact of true nominal biases on complete 3D position (horizontal and vertical).

During the ARAIM performance evaluation, we also defined a term that we called the Safety Index, defined as

$$SI = \frac{|VPE_{nb}|}{\delta VPL}$$

where $\delta VPL = VPL(B_{nom,i}) - VPL(0)$ is meant to reflect the component in the VPL which is designed to bound the ARAIM user position error against the presence of the nominal biases.

There are different options for describing the ARAIM user receiver knowledge of nominal biases.

Whatever the configuration, the ARAIM user xPE is impacted by the true value of the nominal biases, and the VPE also has to be properly bounded by the 10^{-7} fault free bound noted $VAL_{FF}=10m$, and by the composite mode $VAL=35m$.

This was evaluated by checking at all space and time points that

$$VFOM = \sqrt{VPE_{nb}^2 + (K_{FF} * \sigma_V)^2} < VAL_{FF} = 10m$$

Also, it needs to be reminded that the Constellation Service Provider (CSP) navigation message, or the possible online ARAIM overlay navigation message, are currently not providing any reference nominal biases, but the CSP or the online ARAIM navigation message correction parameters (in particular the SV clock parameters) reflect the tracking biases of the CSP (P1/P2 for GPS, E1/E5b for GALILEO), or online ARAIM monitoring stations. Therefore, part of the nominal biases are individually corrected by the CSP navigation (or online ARAIM overlay) message, but the exact amount of the correction brought is not known in general. However,

in the situation of an online ARAIM configuration, ground and airborne constraints could be placed so that the online ARAIM ground station receivers would have configurations similar or close to the ARAIM user receiver configurations. In the simulations conducted, we assumed that the ARAIM user receiver is affected by the nominal biases presented before, but we considered the worst-case situation where the ARAIM user receiver is not getting any correction for these biases.

The ISM is providing for B_{nom} , usually assumed as identical for all SVs, used for xPLs computation. The ARAIM user xPLs depend on the value of known B_{nom} .

So we can identify the following two options:

- Option 1: The ARAIM user Rx only gets a single B_{nom} for all SVs.
- Option 2: Individual reference nominal biases $B_{nom,i}$ are known by the ARAIM user receiver

Note that in option 2, in order to reflect the

Note also that the current ISM B_{nom} parameters are used for xPL computation, but are not meant to be used to correct ARAIM user range measurements for nominal biases. Rather, nominal biases could be at least partly corrected through the clock corrections provided by the CSP or online ARAIM navigation messages, but this is not considered in the evaluation provided in this paper. This choice was made to reflect a situation where online ARAIM is not implemented, and CSP clock corrections do not correct these biases.

EVALUATION OF ARAIM USER PERFORMANCE

We first remind here the results of the evaluation conducted in [Macabiau et al, 2014], when injecting the 3 possible biases as modeled in [Macabiau et al, 2014]. It needs to be noted that the model for nominal signal deformations was slightly different in [Macabiau et al, 2014] than in the current paper, and the model adopted in the current paper may be more extreme.

In [Macabiau et al, 2014], the bias due to nominal signal deformations was shown to have the largest influence on the VPE.

Also, the largest $Safety_Index_nb$ was equal to 0.76, for $B_{nom}=0.75$ m. The largest $Safety_Index_nb$ was 1.14, for $B_{nom}=0.5$ m. The largest $Safety_Index_nb$ was 2.28, for $B_{nom}=0.25$ m.

As a conclusion, $B_{nom}=0.75$ m was leading to a proper VPL bound for our simulations.

Initial tests (not reported) with an offset space grid, and with a different time grid show us the grid would need refinement.

Initial results also had shown that $BW=4\dots20$ MHz and $Cs=0.01\dots0.24$ do not lead to a significant change on VPE_{nb} and $Safety_Index_nb$.

For a proper calculation of VPL_{nb} against nominal biases, the input ISM B_{nom} cannot be the strict value of nominal biases (essentially because the nominal biases are absorbed partly in GPS and GAL user clock offsets).

We ran 19 new simulations with the settings as presented below:

Common settings
User grid: Lat: [-75°;+75°]; Lon: [-180°;+180°]
Time grid: 10 days, step=10 min
Mask angles (5°), 24GPS, 24 GAL, L1/E1 + L5/E5a Signals, UERE (tropo, mult, noise, URA=1m, URE=0.5m)
Threat Model ($P_{sat}=P_{const}=10^{-5}$, $P_{fa}=4\times 10^{-6}$)
[BW;Cs] for L5/E5a: [24MHz;1]

Table 3: Common simulation settings.

Specific Settings
Computation of Nominal bias: Nom Sig + SV grp del
<ul style="list-style-type: none"> • Nom Sig def biases: Values of [BW; Cs] for L1/E1 in regions described before; • User antenna grp delay variation: not injected as assumed to be a low-pass random process covered by $\sigma_{multipath}$
Input ISM B^i:
<ul style="list-style-type: none"> • $B_{nom}=0.75$m in option 1 • Ref B_{nom}^i from nom sig def in option 2 (used to compute xPLs)

Table 4: Specific simulation settings.

This leads to the evaluation of performance at $3.26 \cdot 10^6$ space time grid points. Note however that as the nominal biases are not modeled as random, the main objective of these evaluations is to find the worst-case protection situation.

Figure 36 shows the safety index in option1 where the reference biases are unknown by the user ARAIM Rx (a single $B_{nom}=0.75$ m is provided), $User=24$ MHz-0.12.

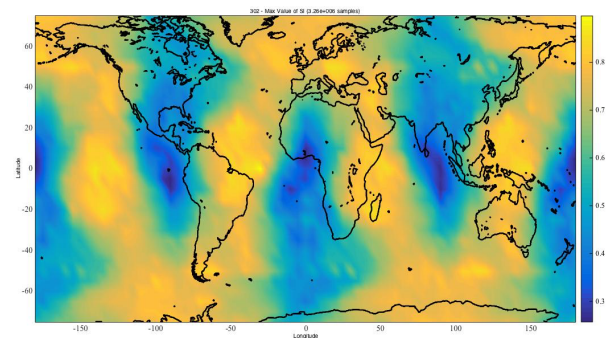


Figure 36: Illustration of maximum safety index for nominal bias VPL bounding, for reference biases

unknown by the user ($B_{nom}=0.75m$), $User(L1)=24MHz-0.12$.

We can see in figure 36 that the largest value of the safety index is equal to 0.90, while the mean value of the safety index is equal to 0.14.

The availability, when evaluation the VPL against $VAL=35m$, and the VFOM against the $VAL_{FF}=10m$, was evaluated to be 100%.

Figure 37 shows the value of the safety index for all BW-Cs configurations previously identified.

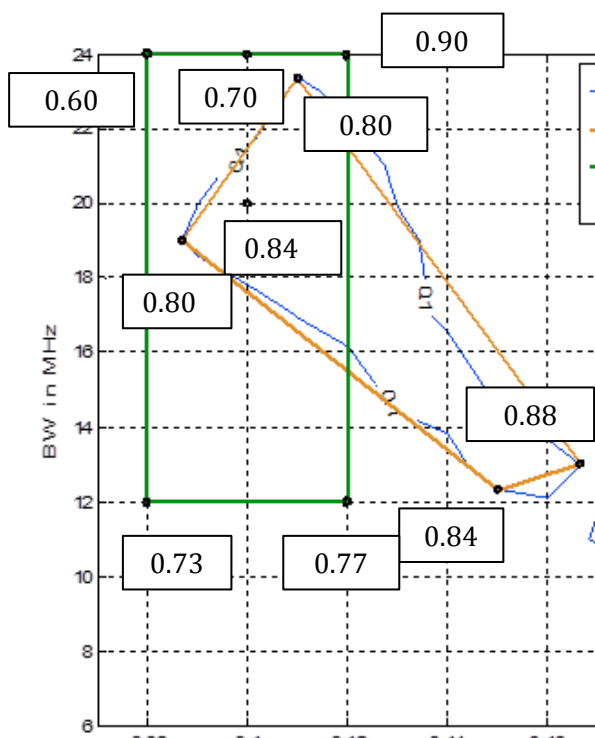


Figure 37: Illustration of safety index for nominal bias VPL bounding, for reference biases unknown by the user ($B_{nom}=0.75m$).

As we can see in figure 37, the 0.1m bounding region previously identified leads to safety indices in 0.8...0.88, and generally speaking values of the chip spacing larger than 0.12 lead to extreme situations.

Figure 38 shows the safety index in option2 where the reference biases due to nominal signal deformation are provided to the user ARAIM Rx, $Ref=24MHz-0.1$ $User=24MHz-0.12$.

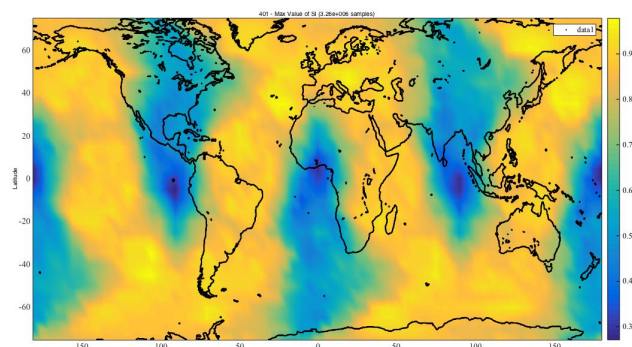


Figure 38: Illustration of maximum safety index for nominal bias VPL bounding, for reference biases unknown by the user ($B_{nom_i}=nom\ sig\ def\ B_{nom_i}$), $Ref(L1)=24MHz-0.1$ $User(L1)=24MHz-0.12$.

We can see in figure 38 that the largest value of the safety index is equal to 0.98, while the mean value of the safety index is equal to 0.16

The availability, when evaluation the VPL against $VAL=35m$, and the VFOM against the $VAL_{FF}=10m$, was evaluated to be 100%.

Figure 39 shows the value of the safety index for all BW-Cs configurations previously identified.

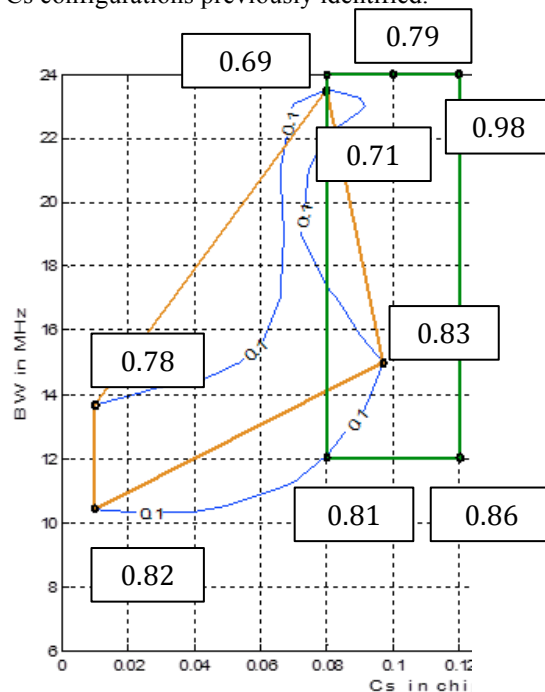


Figure 39: Illustration of safety index for nominal bias VPL bounding, for reference biases known by the user ($B_{nom_i}=nom\ sig\ def\ B_{nom_i}$), $Ref(L1)=24MHz-0.1$.

As we can see in figure 39, the 0.1m bounding region previously identified leads to safety indices in 0.71...0.83, and generally speaking values of the chip spacing equal to 0.12 lead to extreme situations.

Note that the threshold to accept a specific value of safety index due to nominal biases may depend on the assumed

margins in the evaluation of this performance. For example, in the situation where the update rate of the ISM message is very slow (larger than a few years), then margins may be preferable and it would also be preferable to set a threshold for the safety index to 0.75 (similar to the threshold for near MIs in SBAS). In the event where the ISM update rate is faster than a few years, then a threshold of 1 on the safety index may be acceptable.

CONCLUSION

A model for extreme nominal biases due to nominal signal deformation in ARAIM configuration is proposed. These extreme nominal signal deformations are digital deformations taken from Stanford University measurements, and analog deformations taken from a 2nd order model, providing an extreme value plus an extreme dispersion across all SVs of the constellation of the induced tracking error.

The modeled nominal biases due to user antenna group delay variation as a function of azimuth and elevation are taken from an EM model, then proposed to be considered as a random process whose amplitude distribution is overbounded by the $\sigma_{mult} = 0.13 + 0.53e^{-\theta/10}$ m 100s smoothed multipath budget for each L1, L5 E1 OS and E5a measurement.

The adequacy of these models would need to be refined.

With these models, different BW-Cs user receiver configurations were identified using the latest BW-Cs proposal made at RTCA, and using a 0.1m bound on the maximum ranging error due to nominal signal deformations.

Two options for performance evaluations were considered in this paper:

- Option 1: The ARAIM user Rx only gets a single Bnom for all SVs.
- Option 2: Individual reference nominal biases B_{nom}_i are known by the ARAIM user receiver

Note that in none of these options we have considered that the nominal biases are corrected through the CSP message or the possible online ARAIM overlay message. This choice was made to reflect a situation where online ARAIM is not implemented, and CSP clock corrections do not correct these biases.

With our models, when the Bnom provided is a single Bnom=0.75m for all SVs in both constellations, the largest safety index observed is 0.9, which is quite high. Also, chip spacings larger than 0.12 lead to largest values of the safety index.

With our models, when the Bnom provided is the individual Bnom_i equal to the nominal bias due to nominal signal deformation for a reference receiver with BW=24 MHz and Sc=0.1, the largest safety index

observed is 0.98, which is quite high. Also, chip spacings equal to 0.12 lead to largest values of the safety index.

Therefore, from these evaluations, with these settings and with our extreme model for nominal signal deformation, it is recommended that if a single Bnom is provided for all SVs of both constellations, this Bnom needs to be not lower than 0.75m, and possibly larger than 0.75m. If an individual Bnom_i is provided equal to the Bnom_i for nominal signal deformation at a reference receiver configuration BW=24 Cs=0.1, then ARAIM user receiver protection against nominal biases through the VPL is barely achieved when user Cs=0.12.

Note that our preferred solution at this time still is to consider a single Bnom for all SVs for both constellations to cover all possible difficulties to tune an individual Bnom_i per satellite. Another possibility could also be to adopt a single Bnom for all SVs in a constellation but to select a different Bnom per constellation.

Several elements in our model could be refined such as our extreme model for nominal signal deformation, and other options could be evaluated such as the situation where Bnom_i provided in option2 are slightly inflated to reflect more error variation in particular changes or evolutions in the SVs payload configurations, where the user receiver corrects part of the nominal biases through the CSP or online ARAIM message. In addition, the choice to consider the user antenna bias as a random error included in the multipath error could be further analyzed.

Finally, concerning the definition of our simulations, the worst-case situation with a different space-time grid still needs to be searched.

ACKNOWLEDGMENT

The authors would like to gratefully acknowledge CNES for having funded part of this work. However, the opinions expressed in this paper are the author's ones and this paper does not represent a government position on a future development of ARAIM ground segment.

REFERENCES

[EUROCAE, 2013], EUROCAE, Interim GNSS Antenna MOPS, June 2013.

[EUROCAE, 2014], EUROCAE, Minimum Operational Performance Specification for Airborne Open Service GALILEO Satellite Receiving Equipment, version 3.3, March 2014.

[EU-U.S., 2012], EU-U.S. Cooperation on Satellite Navigation, Working Group C, ARAIM Technical Subgroup, Interim Report, issue 1, December 19th 2012.

[FAA, 2010], Phase II of the GNSS Evolutionary Architecture Study, february 2010

[Haines et al., 2012], B.HAINES, W.BERTIGER, S.DESAI, N.HARVEY, A.SIBOIS, J.WEISS, « Characterizing the GPS Satellite Antenna Phase and Group Delay Variations Using Data from Low-Earth Orbiters: Latest Results », 2012 IGS Workshop

[Macabiau et al, 2014], C. Macabiau, C. Milner, Q. Tessier, M. Mabileau, J. Vuillaume, N. Suard, C. Rodriguez, « Impact of Nominal Biases Bounding Techniques on Final ARAIM User Performance », ION ITM 2014

[Milner et al, 2014], Milner C., Macabiau C., Dulery C., Mabileau M, Suard N., Rodriguez C., Pujol S., « An Analysis of ARAIM Performance Sensitivity to the Ground System Architecture Definition », ION GNSS+2013

[Murphy et al., 2007], T.MURPHY, P.GEREN, T.PANKASKIE, « GPS Antenna Group Delay variation Induced Errors in a GNSS Based Precision Approach and Landing Systems », ION ITM 2007

[Phelts et al., 2009], E. PHELTS, T. WALTER, P. ENGE, « Characterizing Nominal Analog Signal Deformation on GNSS Signal », ION GNSS 2009

[Phelts et al., 2013], E. PHELTS, G.WONG, T. WALTER, P. ENGE, « Signal Deformation Proposal », RTCA WG-2, october 8-9 2013

[Phelts et al, 2014a], E. Phelts, T. Walter, P. Enge, « The Effect of Nominal Signal Deformations on ARAIM Users », ION ITM 2014

[Phelts et al., 2014b], Proposal for BW-CS configurations, 2014

[Walter et al, 2012], Walter T., Blanch J., and Enge P., « A Framework for Analyzing Architectures that Support ARAIM », ION-GNSS 2012

[Wong et al., 2010], G. WONG, E. PHELTS, T. WALTER, P. ENGE, « Characterization of Signal Deformations for GPS and WAAS Satellites », ION GNSS 2010

[Wong et al., 2011a], G. WONG, E. PHELTS, T. WALTER, P. ENGE, « Alternative Characterization of Analog Signal Deformation for GNSS-GPS Satellites », ION ITM 2011

[Wong et al., 2011b], G. WONG, E. PHELTS, T. WALTER, P. ENGE, « Bounding Errors Caused by Nominal GNSS Signal Deformations », ION GNSS 2011